NASA Contractor Report 191071
AIAA–92–3672

IN-25
150451
P.18

Computation of H2/Air Reacting Flowfields In Drag-Reduction External Combustion

H.T. Lai
Sverdrup Technology, Inc.
Lewis Research Center Group
Brook Park, Ohio

NASA
National Aeronautics and
Space Administration

(NASA-CR-191071) COMPUTATION OF
H2/AIR REACTING FLOWFIELDS IN
DRAG-REDUCTION EXTERNAL COMBUSTION
(Sverdrup Technology) 18 p

N93-20237

Unclas

G3/25 0150451

COMPUTATION OF H2/AIR REACTING FLOWFIELDS
IN DRAG-REDUCTION EXTERNAL COMBUSTION

H. T. Lai*
Sverdrup Technology, Inc.
NASA Lewis Research Center Group
Cleveland, Ohio 44135

ABSTRACT

Numerical simulation and analysis of the solution are presented for a laminar reacting flowfield of air and hydrogen in the case of an external combustion employed to reduce base drag in hypersonic vehicles operating at transonic speeds. The flowfield consists of a transonic air stream at a Mach number of 1.26, and a sonic transverse hydrogen injection along a row of 26 orifices. Self-sustained combustion is computed over an expansion ramp downstream of the injection and a flameholder, using the recently developed RPLUS code. Measured data is available only for surface pressure distributions, and is used for validation of the code in practical 3D reacting flowfields. Pressure comparison shows generally good agreements and the main effects of combustion are also qualitatively consistent with experiment.

INTRODUCTION

Results obtained from a three-dimensional computation of hydrogen-air combustion are presented for flowfields simulating an external burning experiment [1], which was performed to study external combustion as a mechanism for drag reduction in aerospace vehicles when operating in the transonic regime. The paper presents an analysis of the numerical solutions computed to validate the recently developed RPLUS code. The feasibility of the proposed concept for drag reduction is not of primary concern in this paper, but qualitative conclusions however can be drawn from the results for certain prominent effects of combustion.

One of the important components in hypersonic vehicles is the nozzle which must be designed to operate in a wide range of flow regimes. At the on-design hypersonic conditions, considerably large area ratios are required to accommodate for the extremely high pressure ratios needed to obtain rapid expansion to hypersonic Mach numbers [2,3]. Due to weight consideration of such area ratio requirement, the aft-end of the aircraft is utilized as the expansion surface for the upper nozzle wall. The other lower surface must also be truncated, producing a shear layer between an internal plume exhaust and an external ambient flow. In the transonic regime which occurs at low speed off-design conditions, the nozzle becomes severely overexpanded [3], leading to negative thrust or nozzle drag. One possible means to reduce the internal overexpansion is to use variable nozzle geometry by deflecting the truncated surface. Although the nozzle drag then can be reduced, a base drag, however, is created as a consequence of the ambient flow expansion on the external side of the truncated surface. External combustion is, therefore, proposed as a mechanism to remove this base drag and to affect favorably the exhaust plume in order to achieve fully expanded flowfields. In ref. [1], an analysis of the potential impact of the external burning concept has been presented, and an experiment has also been conducted to study combustion if it is attainable under the transonic conditions.

The experimental configuration consists simply of a small segment of a flat plate connected to a 12-degree expansion ramp, see fig. (1). Over these three-dimensional surfaces, an air stream flows at a supersonic Mach number of 1.26 measured at the leading edge. A sonic transverse injection of hydrogen fuel is located along a row of 26 orifices placed in front of the expansion corner. Downstream of the injection on the flat plate, a rectangular block to be used as flameholder is installed with the trailing edge positioned at the expansion corner. The flameholder has a small opening at the symmetry plane necessary for thermal expansion. The described geometry can be viewed as a combined representation of an external undersurface of the truncated nozzle wall and a

---

*Research Engineer, member AIAA

1

shear layer occurring between the exhaust and ambient flows.

The overall flowfield contains a leading edge shock wave and a downstream Prandtl-Meyer expansion fan in the absence of combustion. When there is combustion. the expansion fan is weaken or eliminated, which is the desired effect making the external air stream to flow without turning at the corner.

At a Mach number of 1.26, the leading edge shock normally detaches because of the boundary layer. More importantly, due to the experimental setup, the underside of the model is a compression surface also inclined at a 12-degree angle. The surface then produces a high pressure region below the model, causing further shock detachment from the leading edge. Consequently, a considerably strong upwash at the leading edge is observed in the experiment. The incoming stream therefore is not parallel to the flat plate but flows locally at an angle of attack near the leading edge. Simulating this effect is costly for the full model since the computational domain becomes rather large. A uniform supersonic profile at Mach 1.26 is then assumed here, for simplicity, as inflow condition at the leading edge.

The RPLUS code [4] is employed to calculate the results presented in this paper. Development and validation of the code are still progressing. Currently, turbulence models have not been implemented, and therefore only laminar flows can be calculated. However, significant physical features are reasonably captured in the present computations although turbulence can be incorporated in future work to improve the results quantitatively. The code has a capability of multi-block grids for treating more complicated surface boundaries, such as in regions of the flameholder or the thermal expansion slot in the present geometry where single grids are difficult to generate. To obtain the solution, the code utilizes an LU solver and takes advantage of 2D vectorization on an oblique grid plane of the computational domain. Although the vectorization is coded only for the implicit side of the solver, the overall procedure can lead to an efficient alternative for calculating, particularly, reacting flows.

Some of the recent works on complex 3D reacting flows using the RPLUS code have been documented for supersonic combustors [5] and for a hydrogen fueled ramjet engine [6], where the flows occur generally in the supersonic regime. This paper illustrates another validation case through an application of the code to practical reacting flowfields in the tran-sonic regime.

NUMERICAL METHOD

The RPLUS code solves for the solutions of the full compressible Navier-Stokes and species equations in a curvilinear coordinate system. A finite volume scheme is formulated in the discretization of the governing equations. The method is second order accurate on a uniform grid, equivalent to using central differences in finite difference formulations. Jameson-type artificial dissipations must also be added to avoid numerical oscillation and instability. For the solutions, an iterative LU algorithm is employed, requiring only scalar inversions of the flow equations but block diagonal inversions of the species equations because of the chemical source terms. All variables are dimensional.

Finite-rate chemistry of hydrogen and air is based on a combustion model containing 18 reaction steps involving 9 species with nitrogen assumed inert. The gas mixture is taken to be thermally perfect. Specific heat, thermal conductivity and viscosity are curve-fitted by fourth degree polynomials of temperature for each species. Mixture specific heat is evaluated by species mass concentration weighting, while mixture thermal conductivity and viscosity are obtained from Wilke's mixing rule. Binary diffusion coefficient is computed based on Chapman-Enskog theory using Lennard-Jones potential functions. More detailed description of the RPLUS code can be found in ref. [4].

GEOMETRY AND GRID

Figure (1) schematically illustrates the experimental geometry and the corresponding system of coordinates. The model has a total length of 36.07 cm and a width of 15.24 cm. The flat plate section is 7.62 cm in length measured from the leading edge, and the following ramp is inclined at an angle of 12 degrees. The flameholder with a trailing edge at the corner juncture has a narrow length of 0.635 cm and a height of 0.318 cm, and it is disjointed in the middle by the small thermal expansion slot having 0.318 cm in width. Hydrogen fuel is sonically injected along a row of 26 circular orifices, which is located at 1.27 cm

in front of the expansion corner. These orifices are uniformly distributed across the model width, each having a diameter of 0.064 cm. The experimental pressure probes are positioned along the symmetry plane.

The corresponding numerical simulation has the inflow and outflow boundaries which coincide with the leading edge of the flat plate and the trailing edge of the expansion ramp respectively. Shock detachment is therefore not allowed since the flow in front of the leading edge is not included in the computational domain. Similarly, the wake downstream of the expansion ramp is also not simulated.

Only one half of the model needs to be computed in the z direction, and one of the boundaries in this direction is the symmetry plane. The computational domain taken in the present work includes the region exterior to the model side edge. The second boundary is then a farfield uniform flow. In the y direction, the upper boundary is located at a distance sufficiently far from the surface so that an undisturbed freestream can be prescribed. The lower boundary coincides with the bottom edge of the model.

A grid representative of the described computational domain is depicted in fig. (2), illustrating surface and boundary grid distributions. Only parts of the inflow, symmetry and lower boundaries are shown, for clarity. Large grid density across the model width is required to resolve the injection orifices. Similarly in the x direction, grid concentration occurs at the injection and around the flameholder. A close-up view of the region around the expansion corner is presented in fig. (3), showing the grids for the rectangular-block flameholder, the thermal expansion opening between one end of the flameholder and the symmetry plane, and a series of the injection orifices indicated by the very small shaded surfaces. The experimental circular orifice is numerically modeled as a square which has the same surface area to obtain the same injected mass flow rate. Each orifice is approximated by two grid cells in the x direction and one cell in the z direction. For gradual distribution, several grid points are also needed in the space between the injectors. A large grid size is therefore required to resolve all 13 orifices for one half of the full model, and consequently the computation time becomes considerable for reacting flows. Although grid refinement for the injectors is possible, no attempt is made here in this regard since demand for computation time with such further refinement is exceedingly high.

Two types of multi-block grids have been used for the computations. One is the internal blocking which is inherent in the RPLUS code and is formulated for complex geometries where the computation domain is divided into several blocks defined by the surface contours. This type of blocking is used to simulate the flameholder and the thermal expansion slot. The other is the external blocking by separating the zones of combustion, which takes place near the ramp surface, and nonreacting flow, which occurs above the combustion zone and extends into the inviscid region. The partitioning is simple since grid coordinates between the two zones are matched identically, although mismatched grid can also be constructed and has been used in ref. [5]. Presently, the use of matched grids allows straightforward transferring of solutions at the interface without the need for interpolation. Interaction between the two zones is iteratively performed external to RPLUS. The main purpose of external blocking is to reduce computer time particularly in the nonreacting region since there is only one species, air, to be calculated and convergence can be reached much faster than in the combustion zone. External blocking is also utilized here in order to place the upper boundary at a distance far above the ramp surface with coarse mesh distributions.

The total grid has a dimension of 48x50x96, with the largest dimension in the z direction having 84 grid points distributed across the model width. External blocking is used only in the y direction, with 10 grid points in the nonreacting zone near the upper boundary, and 30 points in the combustion zone above the ramp surface. The region exterior to the side edge has 10 grid points distributed from the lower boundary to the ramp surface. The smallest spacing is about 0.0001 cm at the no-slip surfaces, sufficient to resolve the laminar viscous layer.

RESULTS

Two cases of reacting and nonreacting flowfields have been computed for the same flow conditions on an identical grid. The incoming air is provided at a Mach number of 1.26, a temperature of 228 K and a pressure of 0.54 atm. whereas hydrogen fuel is injected at a Mach of 1, a temperature of 228 K and a pressure of 23.8 atm. Because of the low temperature

3

used in both streams, spontaneous chemical reaction of air and hydrogen cannot occur, but the injection leads to a mixing, nonreacting flowfield which does not deviate significantly from the case of pure air flows except in the region near the injection. For self-sustained combustion to take place, some form of heat source must be introduced initially to induce chemical reaction. Experimentally, spark ignition was used but possible only at low subsonic incoming Mach numbers. The air stream was then gradually adjusted to the supersonic condition of Mach 1.26. For the reacting results presented here, combustion is numerically initiated using higher fuel temperature and then reducing it to the desired temperature of 228 K after combustion has already established in the flowfield. An ignition fuel temperature value of 1400 K has been used successfully to achieve the initial induced reaction and the subsequent self-sustain combustion. Results of the mixing and reacting cases are presented and compared in the discussion below.

Figure (4) illustrates a typical streamwise flow pattern in terms of Mach contours in a z-constant plane between the side edge and the symmetry plane for the nonreacting case. Only a portion of the flowfield near the surface is shown and discussed herein. The basic structure contains a very weak leading-edge shock completely diffused by numerical dissipations, and a well-defined expansion fan at the corner. Effects of hydrogen injection are negligible in the inviscid region above the injection, where it consists only of pure air. A small region of separation is also visible behind the flameholder at this particular spanwise (z) location. Fig. (5) depicts a three-dimensional view for Mach contours at various cross-sectional planes. Only subsonic Mach numbers are plotted so that comparisons can be made latter with the combustion case. It can be observed that the flow is highly three-dimensional with the existence of streamwise vortices indicated by two large regions of subsonic flows. The vortex along the symmetry plane is produced because of the thermal expansion slot, while the other, smaller vortex is present due to the geometry and the pressure difference between the ramp surface and the ambient flow.

When there is combustion, the flowfield has a significantly different structure. Mach contours for the reacting case are shown on the same z-plane in fig. (6), and at various x-planes in fig. (7) plotted, again, only for subsonic Mach numbers. Importantly, both of the vortices are diminished and the flow shows two-dimensionality within the model. The inviscid

region above the ramp is markedly altered, containing a weaken expansion fan having a smaller turning angle, and a subsonic zone which increases substantially in size and becomes more uniform across the model width. However, upstream influence of combustion appears to be minimal in front of the flameholder.

The effect of combustion, which is to prevent flow turning at the expansion corner, can be seen by comparing fig. (8) and (9) plotted for the particle traces in the same z-plane used for Mach numbers above. First, it can be seen clearly that the streamline for the noncombustion case is somewhat parallel to the ramp surface because of flow turning. With combustion, the streamline remains nearly horizontal behind the flameholder and it is then shifted upwards in a region near the outflow where combustion is more extensive. Second, combustion enlarges the separated region, as seen in fig. (9). The enlargement of the separated flow also extends in the spanwise direction which can be seen from the next figures (10,11). In the nonreacting case, fig. (10), the separation is centered near the symmetry plane, whereas in the reacting case, fig. (11), the bubble is centered near the side edge, showing separated flows occurring nearly throughout the model width. The streamwise vortex along the side edge is also apparent for the nonreacting flow in fig. (10), evident by the collapsing of the particle traces along the model edge.

Contours for hydrogen mass fraction without combustion are presented in fig. (12). The contour variation shows a fuel distribution which is uniform near the flameholder and then concentrated downstream along the symmetry plane due to the three-dimensional relief effect of the high pressure ambient flow. Typical hydrogen mass-fraction distributions in the streamwise direction for the nonreacting and reacting cases are shown in figs. (13,14) for the same z-plane midway between the symmetry plane and the side edge. Identical contour levels are used in both figures. A sparse concentration of contours far downstream of the flameholder in fig. (14) indicates hydrogen consumption by combustion. Top views of the hydrogen distribution are shown in figs. (15,16) for both cases, showing the relief effect without combustion and a more uniform spanwise variation in the combustion case.

Contours of temperature and mass fraction of water vapor are illustrated in figs. (17,18). Both figures depict a similar pattern where large variations exist across a thick layer above the ramp surface,

4

where high rates of reaction occur. In general, The flow reaches a peak temperature in a region near the outflow and slightly above the ramp surface. Typical top view of temperature contours is presented in fig. (19) at a vertical distance near the ramp surface. The dense distribution along the symmetry plane corresponds to a narrow region originated from the thermal expansion slot, in which the combustion is very weak largely due to high concentration of hydrogen with little mixing. Combustion is more extensive in the interior region having a peak temperature occurring near the side edge at the outflow. Fig. (20) demonstrates the contours for mass fraction of water vapor in several cross-sectional planes. Combustion intensity increases for the flow in regions near the wall where highest concentration of water vapor is produced.

Figure (21) depicts distributions of mass flow rates for hydrogen and some of the species whose productions are relatively high. For hydrogen, comparison is made between reacting and nonreacting. As can be seen, hydrogen mass flow rate remains constant without combustion, while gradual reduction of hydrogen is evident with combustion. Approximately, forty percent of hydrogen is consumed in the case of a laminar flow assumed in the present computation. Water vapor is predominantly present in the combustion products but, for other species, the productions are very small or negligible. The corresponding distributions for mass fraction of chemical species and temperature are shown in fig. (22). The variations represent the maximum values taken at each axial computational plane and then plotted along the ramp length. Mass fraction for water vapor is also prominent in magnitude as compared to those of other species, with a largest value located near the flameholder and a decreasing variation downstream. Axially maximum temperature increases toward the outflow, showing sudden combustion behind the flameholder and continuing reaction accumulated as the flow progresses. The peak temperature of about 2050 K is in agreement with experiment.

Temperature distributions are also plotted in figs. (23,24) for several z-planes from the symmetry plane at $z=0$, to near the model side edge at $z=0.075$. The plotted values are also locally maximum, taken along vertical grid lines at each axial plane. At $z=0$ as in fig. (23), it can be clearly seen that the combustion takes place more gradually than abruptly, consisting of two subsequent temperature rises with strong re-action occurring latter in the second stage initiated from the middle section of the ramp. For the interior region up to $z=0.055$ in fig. (24), the distributions are similar to one another and combustion is rather sudden behind the flameholder. The presence of the flameholder is, therefore, to keep the flame front to attach at the expansion corner rather than downstream as exhibited at the symmetry plane. Regions associated with high temperature are located near the side edge as indicated by the curve at $z=0.064$ in fig. (24). It is noted that this curve is similar to that in fig. (22). Next to this region, the distributions at $z=0.071$ and 0.075 represent the variations at a location corresponding to the spanwise boundary of the combustion zone along the side edge where the reaction starts to diminish.

Comparison with experiment is made in figs. (25,26) for surface pressure distributions along the symmetry plane for both nonreacting and reacting cases. The computed results show qualitatively correct trends of the pressure variations according to measurement. The discrepancy near the leading edge is attributed primarily to the existence of an upwash at the leading edge where experimental data shows a negative pressure coefficient. Apparently, the experimental flow has a local angle of attack at the leading edge, which is critically high to cause a very large pressure drop. The use of a uniform supersonic profile as inflow condition to simplify the simulation also contributes to the discrepancy since effect of shock detachment is not taken into account. There is also disagreement behind the expansion corner, and it is reasonably attributed to the laminar regime which can lead to severe regions of separation associated with adverse pressure gradients. In general, the agreement between computation and experiment is good. considering the flow complexity and the simplifying approximations employed in the simulation. Most importantly, the computed results predict fairly well the effect of combustion, that is to increase pressure on the ramp surface. as can be seen by comparing figs. (25) and (26) particularly near the corner. Note that the peak pressure corresponds to the location of hydrogen injection. Measured pressure in the combustion case remains constant behind the flameholder. whereas computed pressure shows oscillation due to the large region of laminar separation. Surface pressure tends to approach ambient pressure near the outflow. For nonreacting, this recovery is caused by the three-dimensional relief effect previously mentioned. Combustion in the experiment

also exhibits considerable upstream influence up to the leading edge, suggesting that, on the flat plate, there is a thick subsonic region adjacent to the viscous layer or even a reversed flow. This subsonic flow permitting upstream influence is created by the detached bow shock and further affected by the upwash, but is not present in the computed flowfield since a very thin subsonic layer is produced because of a uniform supersonic inflow.

The presented results for the nonreacting case have been converged to a residual reduction of nearly three orders of magnitude. Further reduction is possible but the convergence rate becomes slow. Each iteration takes 14 seconds and the total time is about 100 hours on a YMP computer. For the reacting case, the convergence has been quite difficult and extremely slow. Each iteration requires 45 seconds and the total time is approximately 400 hours for a reduction of only two orders of magnitude. Under-relaxation of the temperature and pressure fields is used. The lack of robustness and consequently the slow convergence rate are likely caused by the chemical source terms, even though partially implicit treatments of these terms in the RPLUS code have reduced some of the inherent stiffness. Another possibility worth mentioning is the outflow conditions. In the reacting case, the subsonic region at the outflow is substantial, and the boundary condition here is not determined unless the wake behind the ramp must also be simulated. Extrapolation as used in the present work can adversely affect the convergence behavior.

SUMMARY

Numerical results obtained from the RPLUS code have been presented for a case of external combustion using air and hydrogen. Both nonreacting and reacting flows in the laminar regime are simulated and surface pressure is compared to experimental data for validation. The agreement between measured and computed pressure is qualitatively good. Most importantly, the effect of combustion, that is to increase the ramp pressure and consequently to prevent flow turning at the expansion juncture, is predicted consistently with experiment.

REFERENCES

1 Trefny, C. J., "On the Use of External Burning to Reduce Aerospace Vehicle Transonic Drag," AIAA-90-1935.

2 Lai, H. T., "3D Computation of Single-Expansion-Ramp and Scramjet Nozzles," Computational Fluid Dynamics Symposium on Aeropropulsion, NASA CP-10045, 1990.

3 Lai, H. T., "3D Computation of Hypersonic Nozzle," AIAA-90-5203.

4 Yu, S., Tsai, Y., and Shuen, J., "Three-Dimensional Calculation of Supersonic Reacting Flows Using an LU scheme," AIAA-89-0391.

5 Moon, Y. J., "Numerical Study of Supersonic Combustors by Multi-Block Grids with Mismatched Interfaces," AIAA-90-5204.

6 Duncan, B., "CFD Analysis of a Hydrogen Fueled Ramjet Engine at Mach 3.44," AIAA-91-1991.

hydrogen injection(26 orifices)

flameholder

air flow

thermal expansion slot

symmetry plane
(experimental pressure probes)
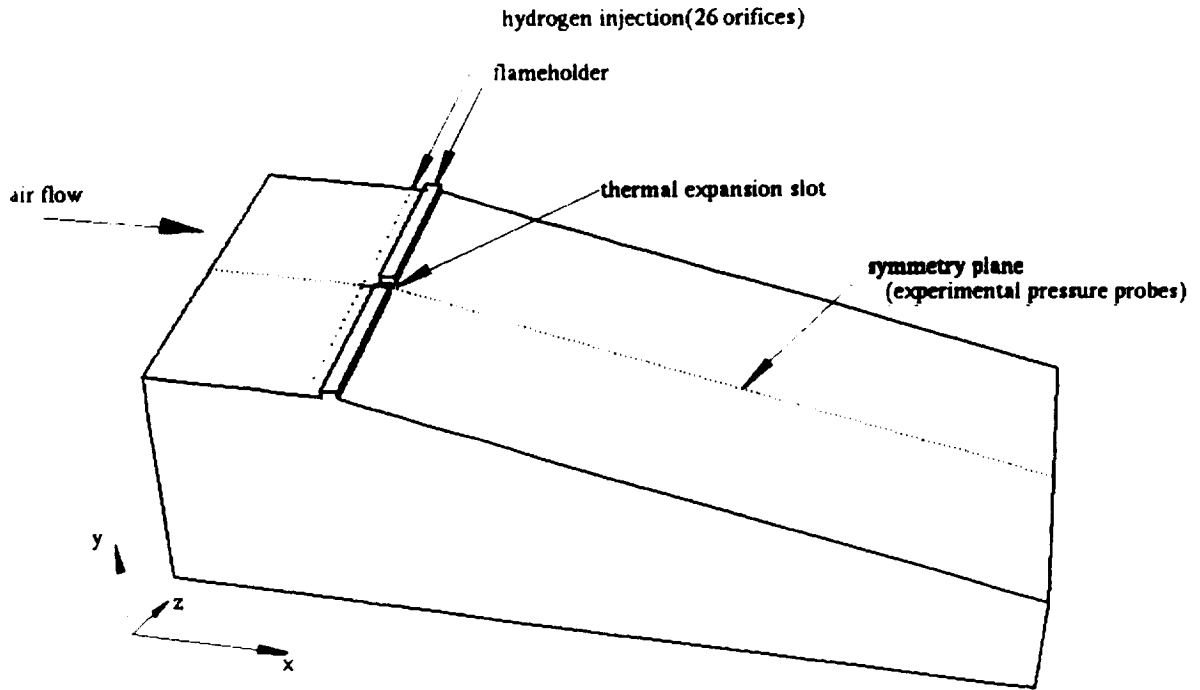
fig. 1   Geometry and coordinate system.

symmetry plane

inflow
boundary

lower boundary
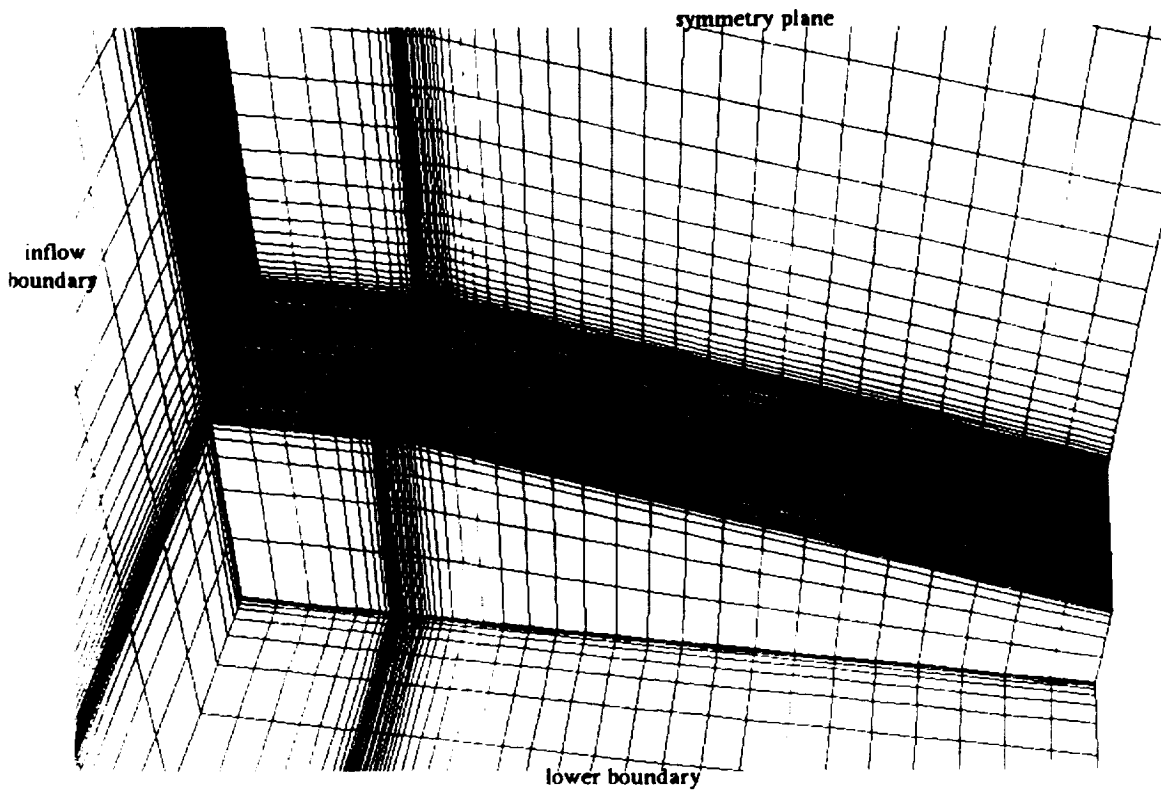
fig. 2   Surface and boundary grid distributions.
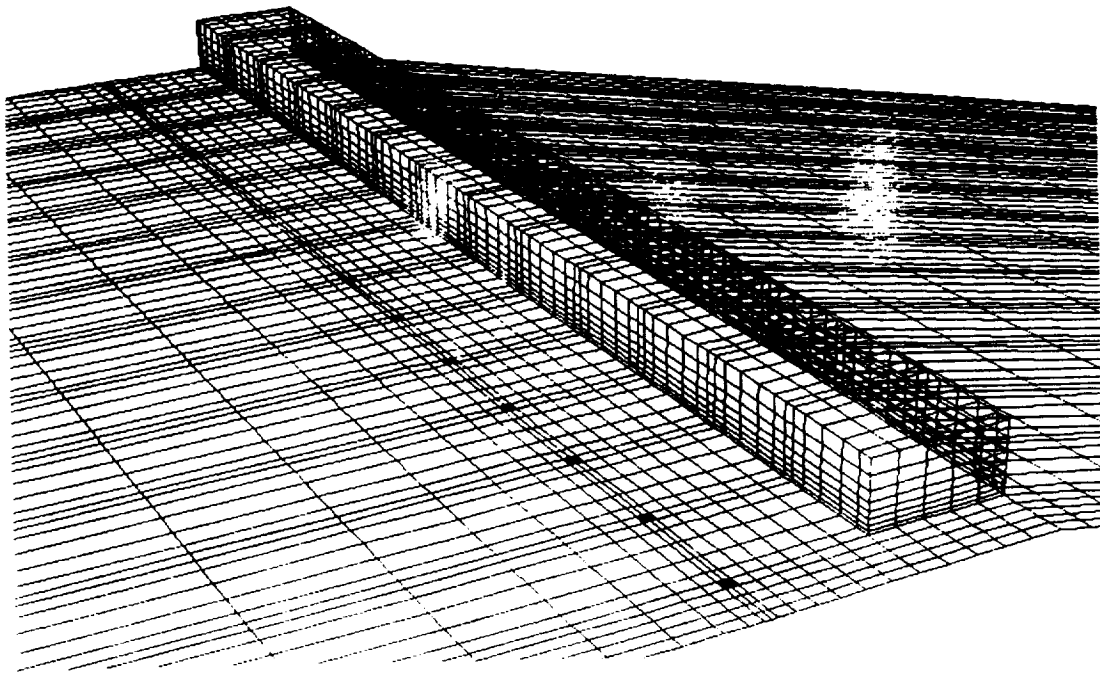
7

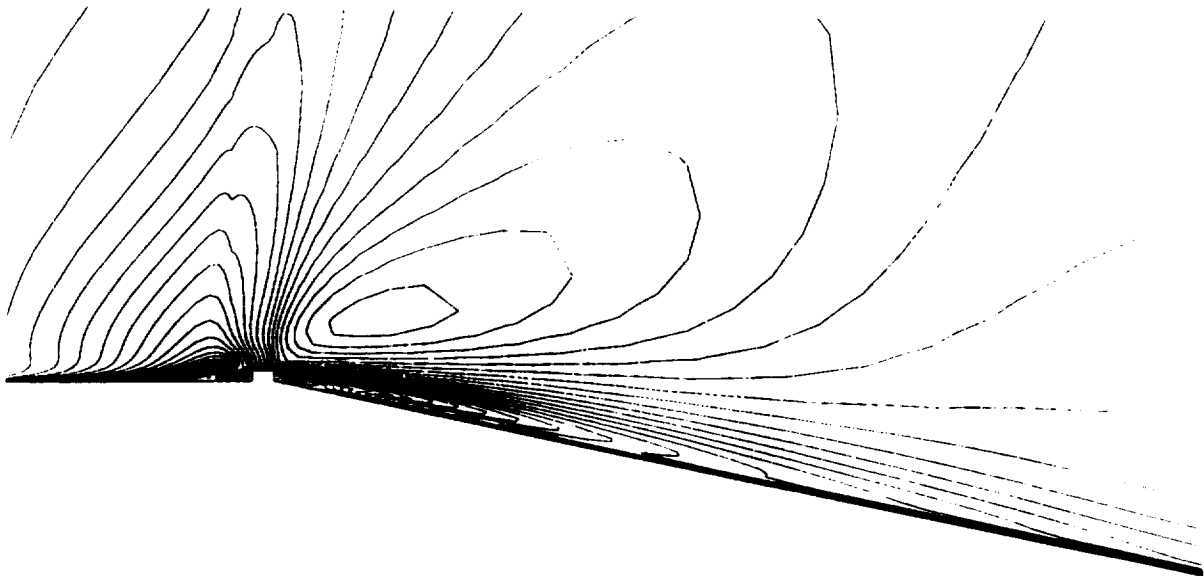fig. 3   Near flameholder grid distribution.
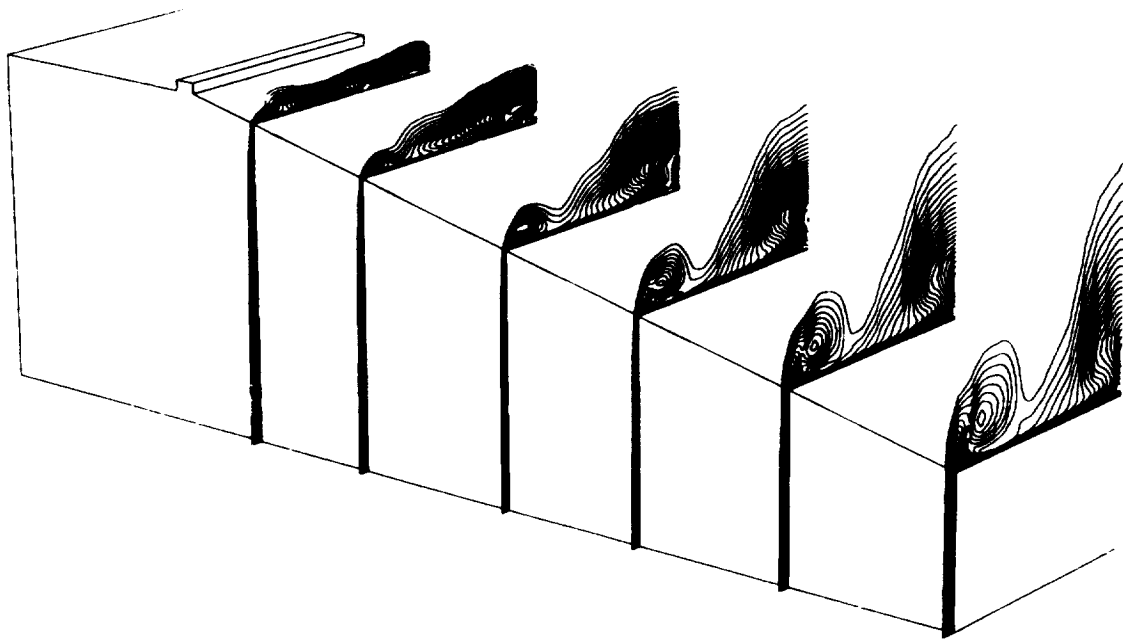

fig. 4   Mach contours, z-plane, nonreacting.
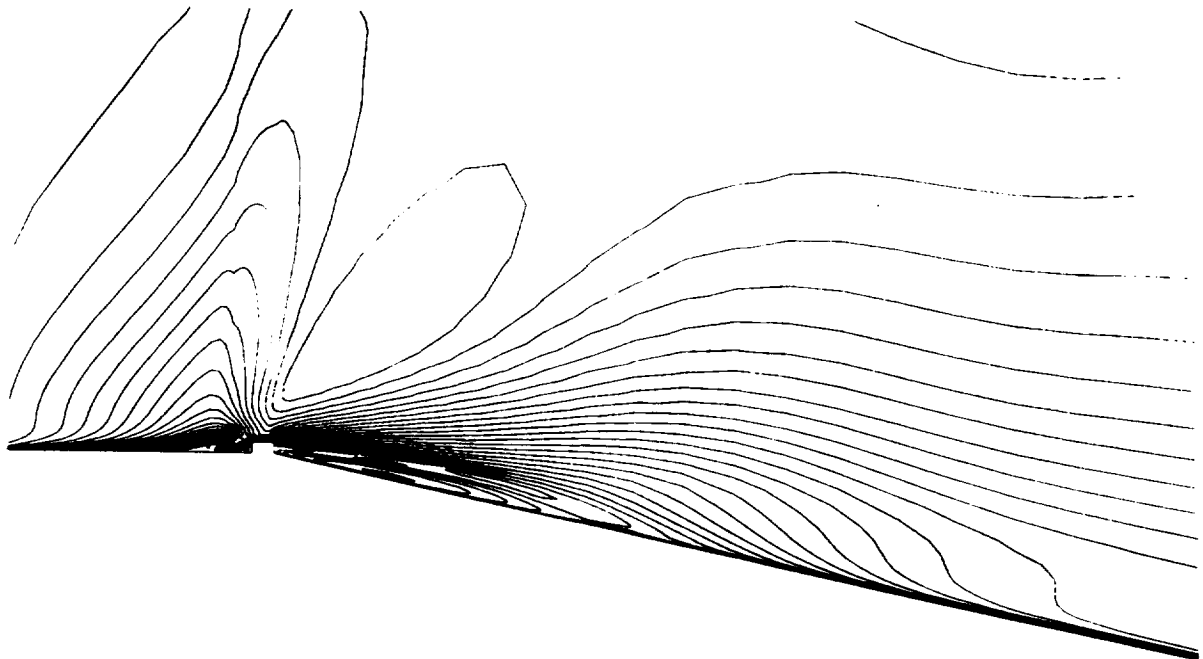
fig. 5   Mach contours, x-plane, nonreacting.
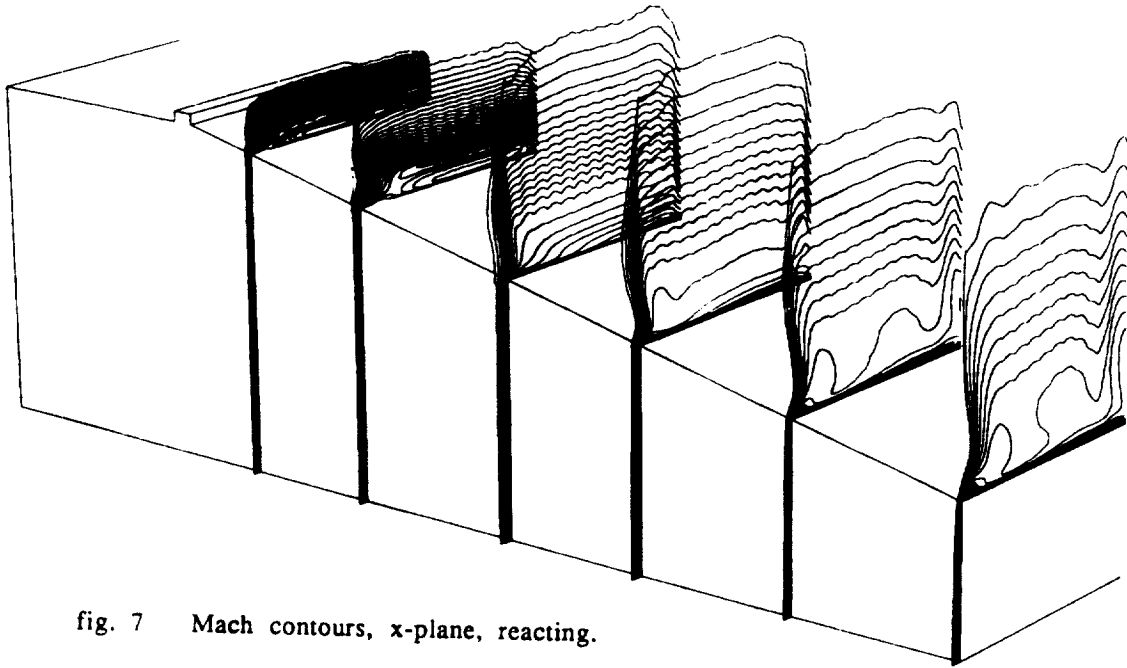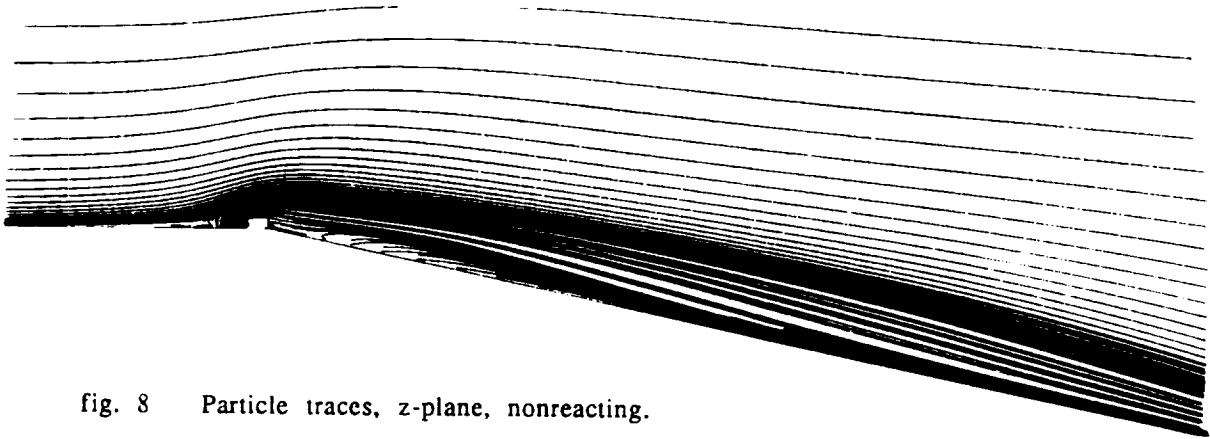

fig. 6   Mach contours, z-plane, reacting.

9

fig. 7   Mach contours, x-plane, reacting.

fig. 8   Particle traces, z-plane, nonreacting.
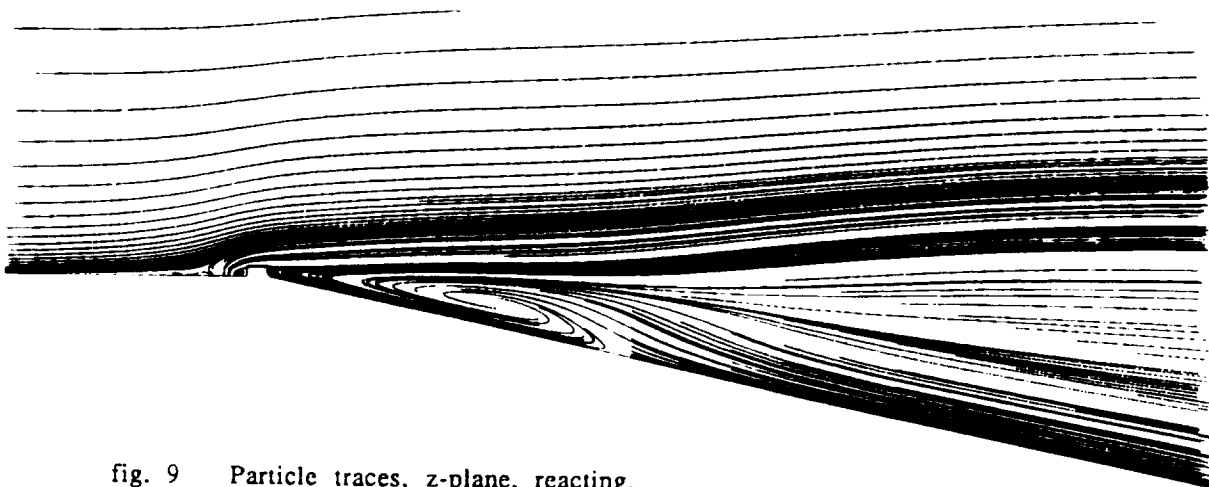
fig. 9   Particle traces, z-plane, reacting.

fig. 10   Particle traces, y-plane, nonreacting.
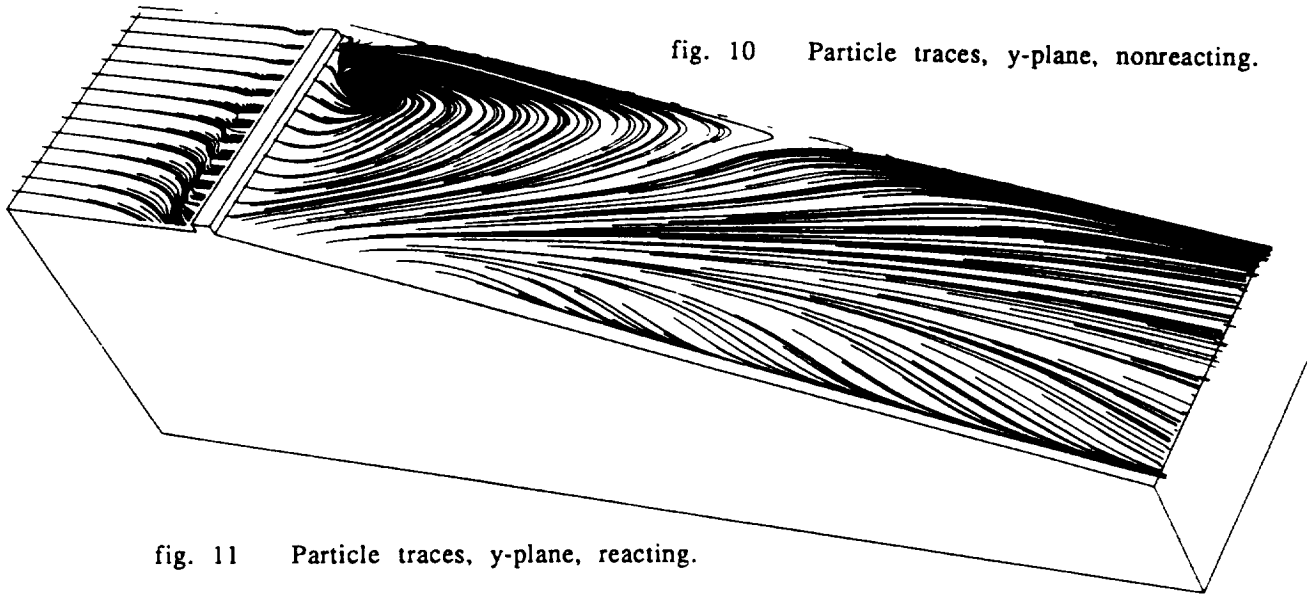
fig. 11   Particle traces, y-plane, reacting.
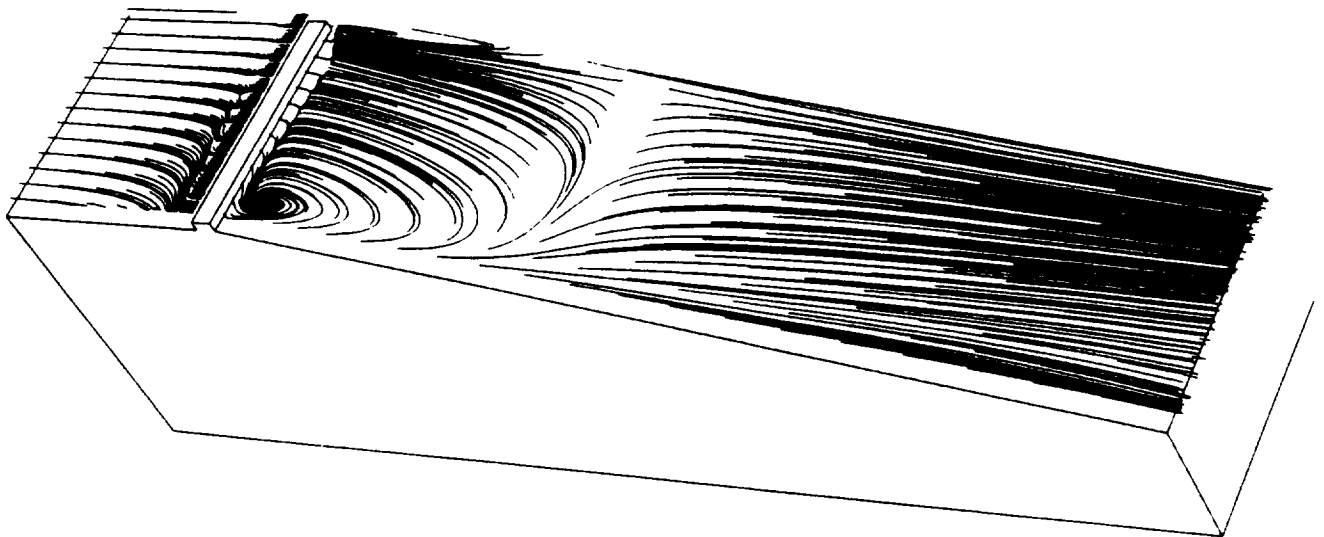
fig. 12   Contours of hydrogen mass fraction, x-plane, nonreacting.
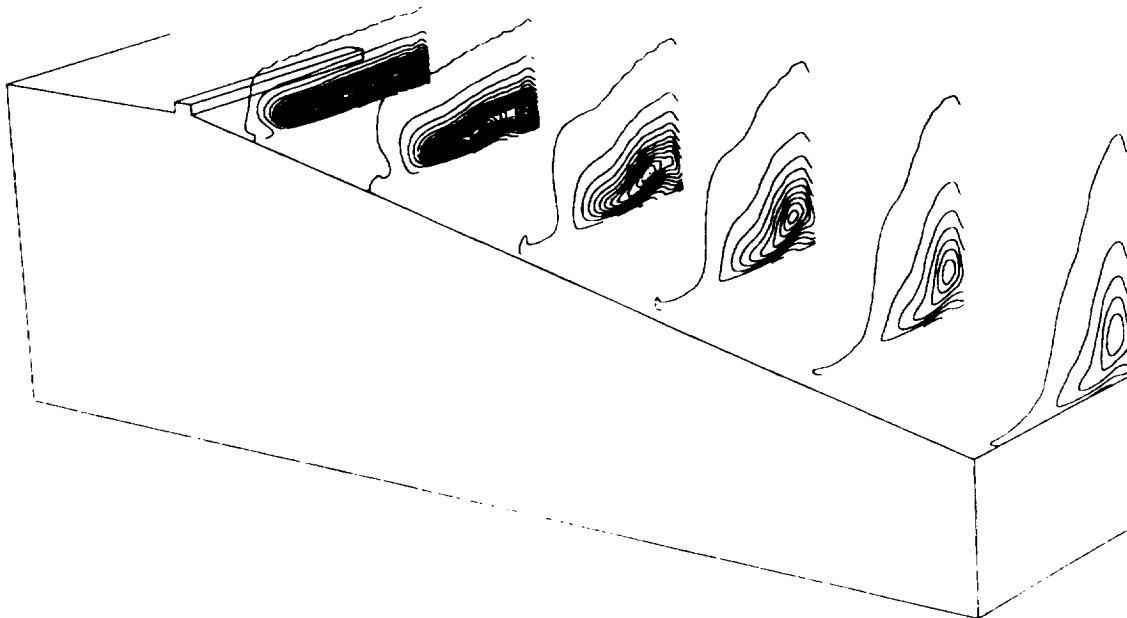
fig. 13   Contours of hydrogen mass fraction, z-plane, nonreacting.
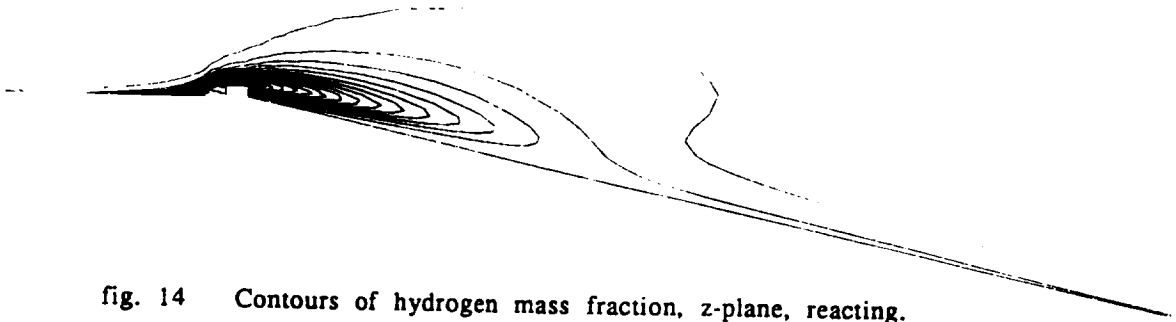
fig. 14   Contours of hydrogen mass fraction, z-plane, reacting.
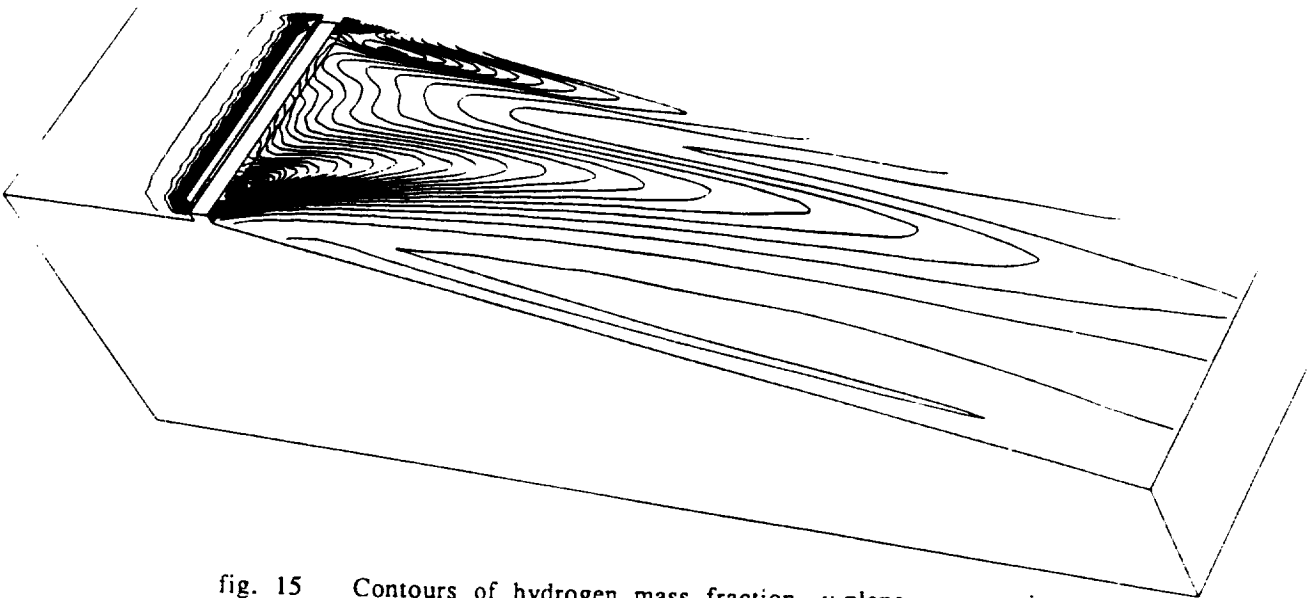
fig. 15   Contours of hydrogen mass fraction, y-plane, nonreacting.
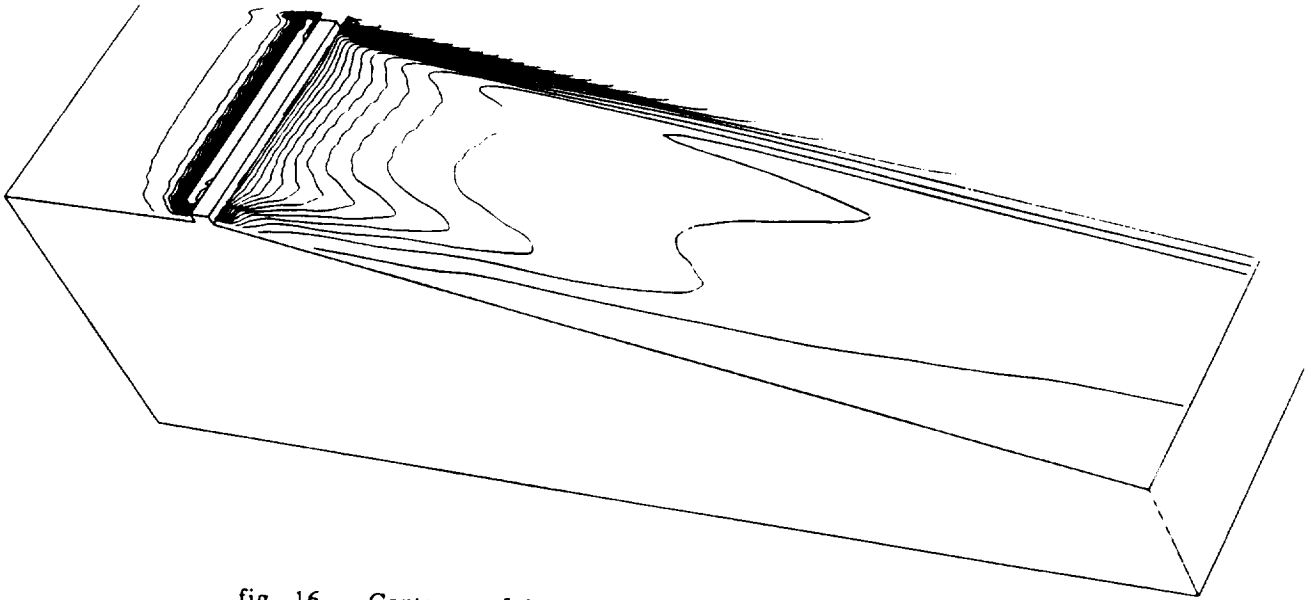
fig. 16   Contours of hydrogen mass fraction, y-plane, reacting.
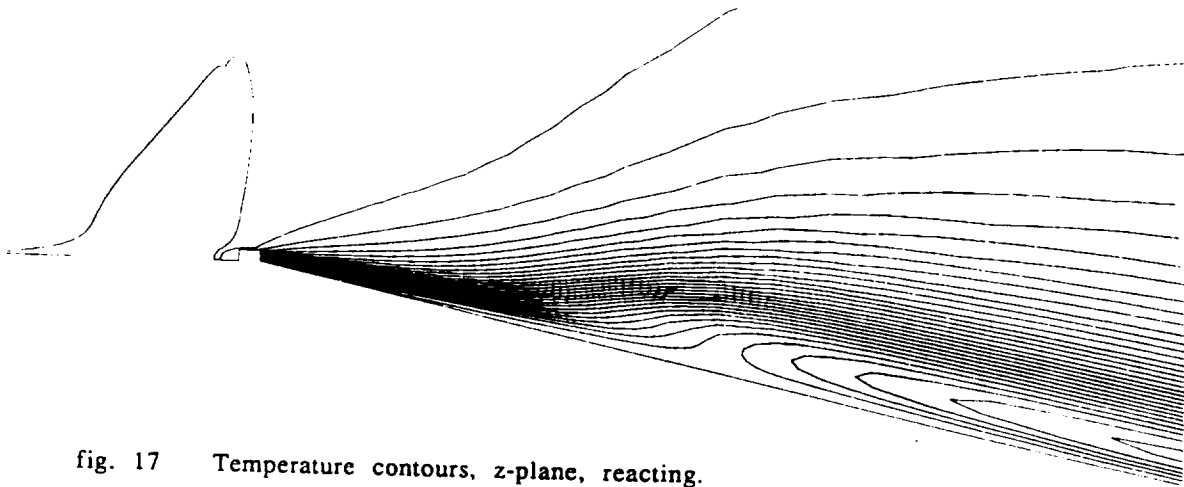
fig. 17   Temperature contours, z-plane, reacting.
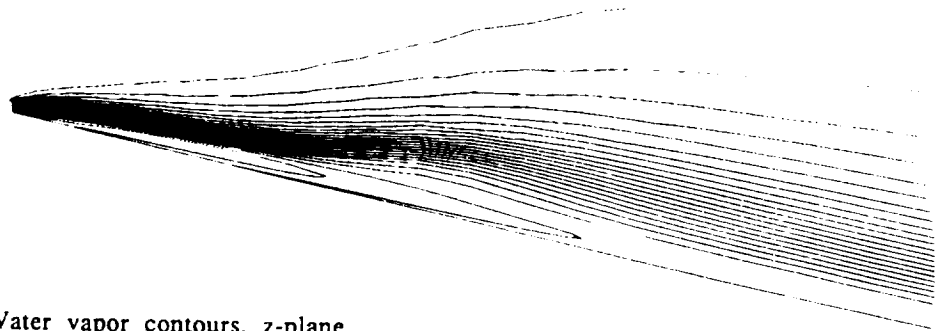
fig. 18   Water vapor contours, z-plane.
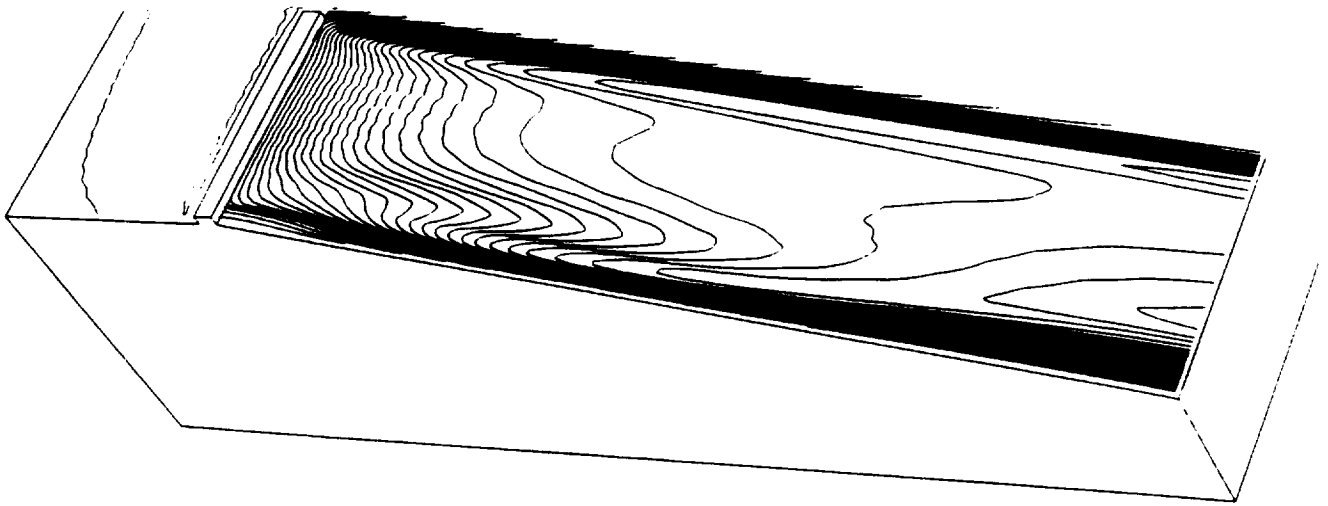
fig. 19   Temperature contours, y-plane, reacting.
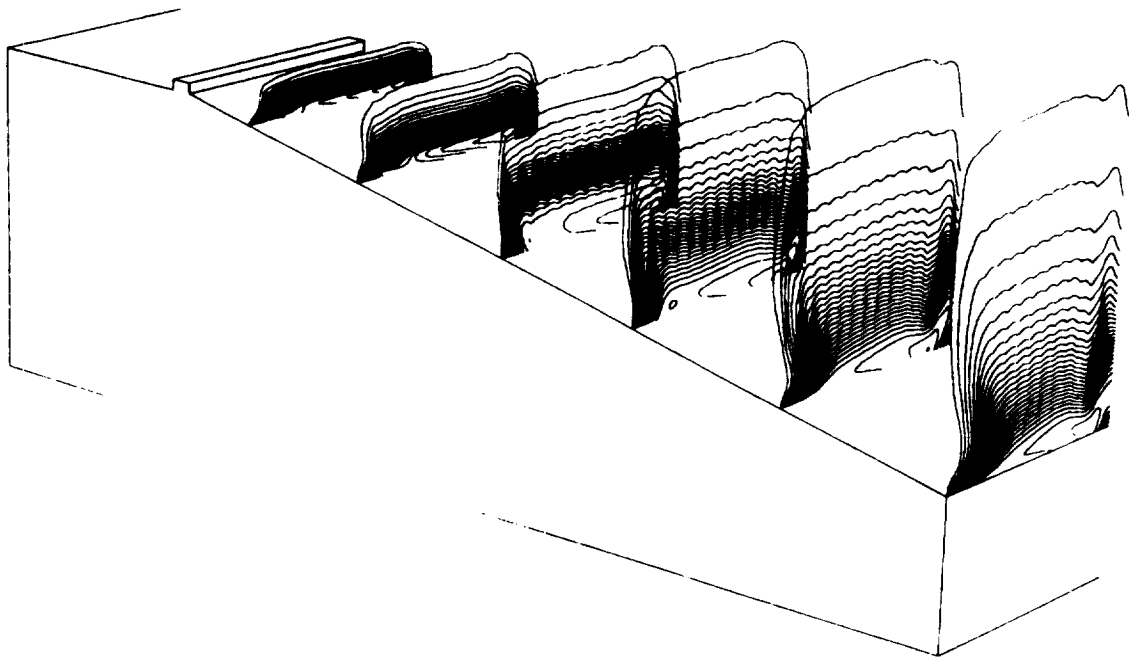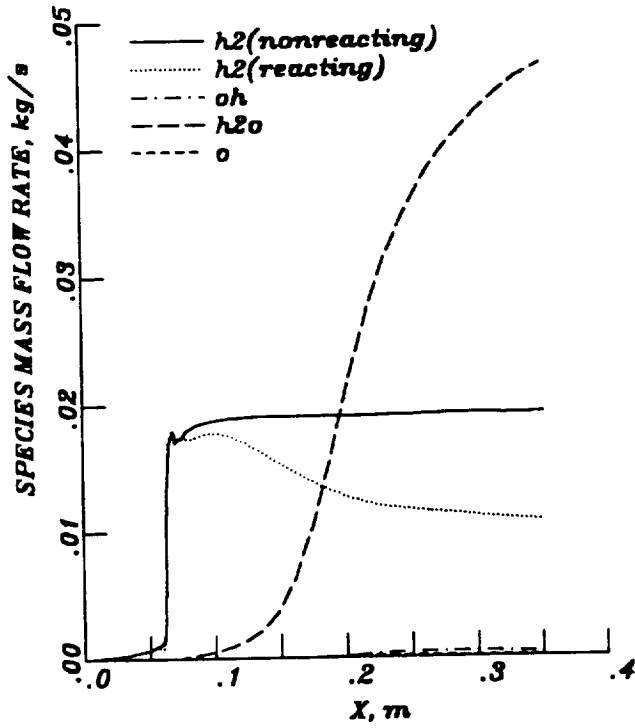

fig. 20   Water vapor contours, x-plane.
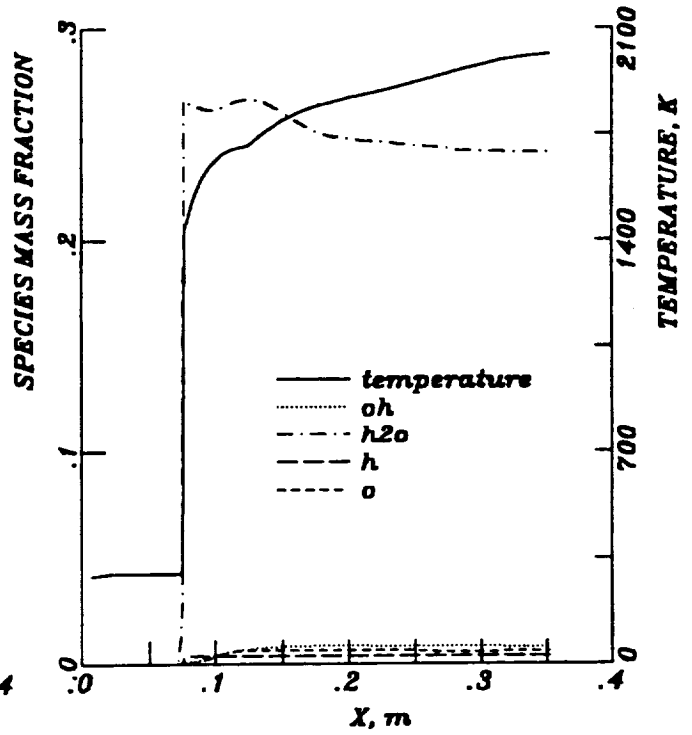
fig. 21　　Distributions of species mass flow rates.

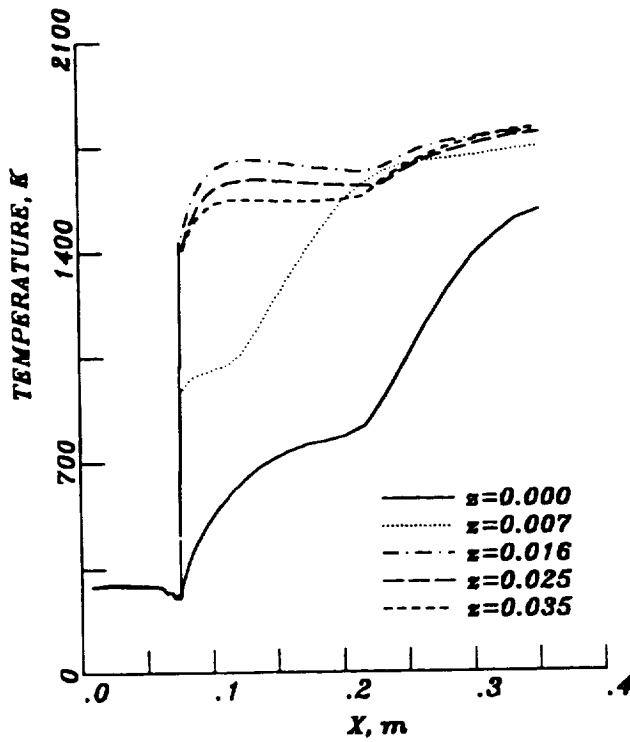fig. 22　　Distributions of species mass fractions.

fig. 23　　Temperature distributions, near the symmetry plane.
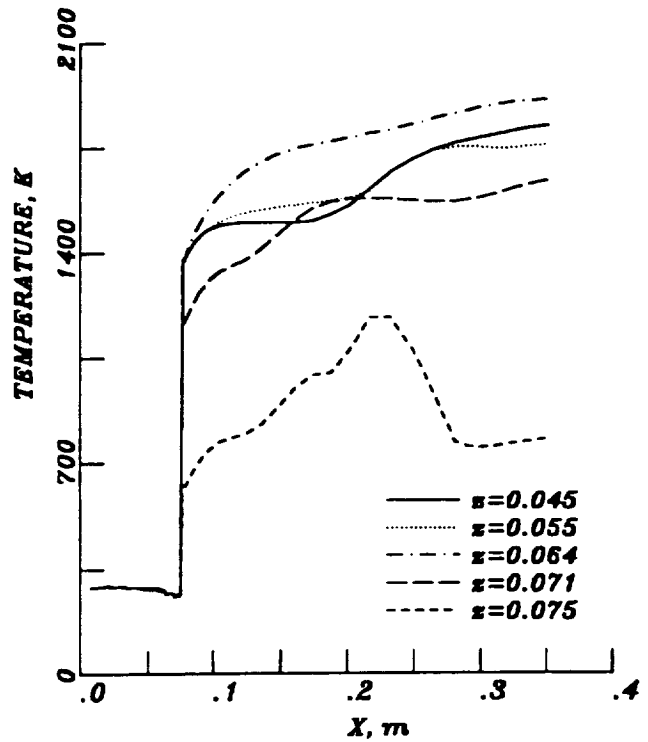
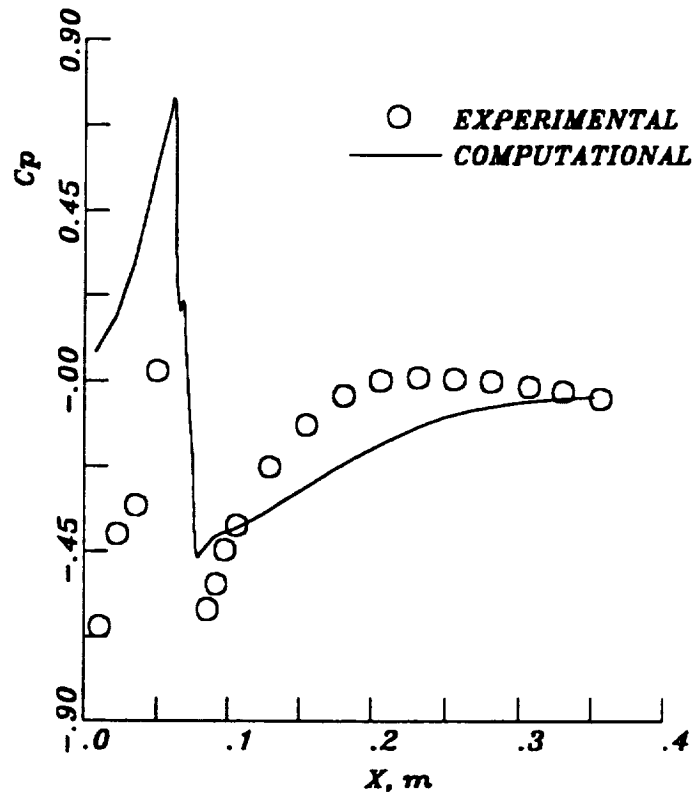fig. 24　　Temperature distributions, near the side edge.

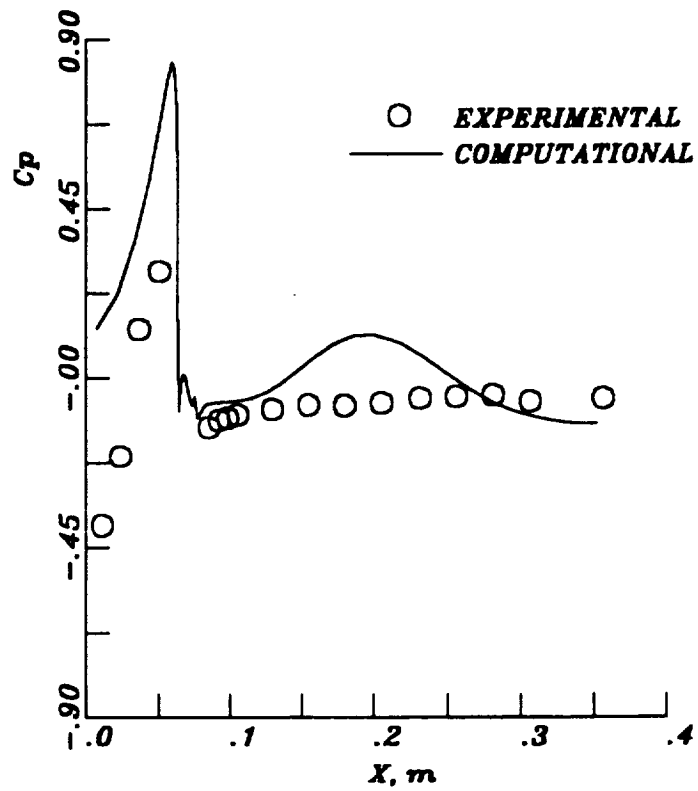fig. 25   Pressure distribution, symmetry plane, nonreacting.

fig. 26   Pressure distribution, symmetry plane, reacting.

REPORT DOCUMENTATION PAGE			*Form Approved* *OMB No. 0704-0188*

Public reporting burden for this collection of information is estimated to average 1 hour per response, including the time for reviewing instructions, searching existing data sources, gathering and maintaining the data needed, and completing and reviewing the collection of information. Send comments regarding this burden estimate or any other aspect of this collection of information, including suggestions for reducing this burden, to Washington Headquarters Services, Directorate for information Operations and Reports, 1215 Jefferson Davis Highway, Suite 1204, Arlington, VA 22202-4302, and to the Office of Management and Budget, Paperwork Reduction Project (0704-0188), Washington, DC 20503.

1. AGENCY USE ONLY *(Leave blank)*	2. REPORT DATE July 1992	3. REPORT TYPE AND DATES COVERED Final Contractor Report	
4. TITLE AND SUBTITLE Computation of H2/Air Reacting Flowfields In Drag-Reduction External Combustion			**5. FUNDING NUMBERS** WU–
6. AUTHOR(S) H.T. Lai			
7. PERFORMING ORGANIZATION NAME(S) AND ADDRESS(ES) Sverdrup Technology, Inc. Lewis Research Center Group 2001 Aerospace Parkway Brook Park, Ohio 44142			**8. PERFORMING ORGANIZATION REPORT NUMBER** E–7624
9. SPONSORING/MONITORING AGENCY NAMES(S) AND ADDRESS(ES) National Aeronautics and Space Administration Lewis Research Center Cleveland, Ohio 44135–3191			**10. SPONSORING/MONITORING AGENCY REPORT NUMBER** NASA CR–191071 AIAA–92–3672

11. SUPPLEMENTARY NOTES

12a. DISTRIBUTION/AVAILABILITY STATEMENT Unclassified - Unlimited Subject Category	**12b. DISTRIBUTION CODE**

13. ABSTRACT *(Maximum 200 words)*

Numerical simulation and analysis of the solution are presented for a laminar reacting flowfield of air and hydrogen in the case of an external combustion employed to reduce base drag in hypersonic vehicles operating at transonic speeds. The flowfield consists of a transonic air stream at a Mach number of 1.26, and a sonic transverse hydrogen injection along a row of 26 orifices. Self-sustained combustion is computed over an expansion ramp downstream of the injection and a flameholder, using the recently developed RPLUS code. Measured data is available only for surface pressure distributions, and is used for validation of the code in practical 3D reacting flowfields. Pressure comparison shows generally good agreements and the main effects of combustion are also qualitatively consistent with experiment.

14. SUBJECT TERMS H2/air combustion; External combustion; Aerospace vehicles; CFD transonic			**15. NUMBER OF PAGES** 18
			16. PRICE CODE A03
17. SECURITY CLASSIFICATION OF REPORT Unclassified	**18. SECURITY CLASSIFICATION OF THIS PAGE** Unclassified	**19. SECURITY CLASSIFICATION OF ABSTRACT** Unclassified	**20. LIMITATION OF ABSTRACT**